Accepted Manuscript

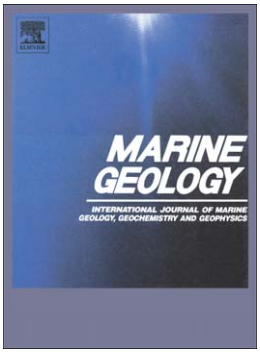

Spectral signatures for swash on reflective, intermediate and dissipative beaches

Michael G. Hughes, Troels Aagaard, Tom E. Baldock, Hannah E. Power

PII: S0025-3227(14)00149-2
DOI: doi: 10.1016/j.margeo.2014.05.015
Reference: MARGO 5114

To appear in: *Marine Geology*

Received date: 7 July 2013
Revised date: 27 April 2014
Accepted date: 24 May 2014

Please cite this article as: Hughes, Michael G., Aagaard, Troels, Baldock, Tom E., Power, Hannah E., Spectral signatures for swash on reflective, intermediate and dissipative beaches, *Marine Geology* (2014), doi: 10.1016/j.margeo.2014.05.015

Spectral signatures for swash on reflective, intermediate and dissipative beaches

Michael G. Hughes[1]
Troels Aagaard[2]
Tom E. Baldock[3]
Hannah E. Power[4]

1. Corresponding author: School of Geosciences, University of Sydney, Sydney NSW 2006 Australia (michael.hughes@sydney.edu.au)

2. Institute of Geoscience and Natural Resources, University of Copenhagen, Copenhagen Denmark

3. School of Civil Engineering, University of Queensland, Brisbane QLD Australia

4. Geoscience Australia, Canberra ACT Australia

Revised Manuscript Submitted to Marine Geology

April 2014

Abstract

In this paper we synthesise a large data set gathered from a wide variety of field deployments and integrate it with previously published results to identify the spectral signatures of swash from contrasting beach types. The field data set includes the full range of micro-tidal beach types (reflective, intermediate and dissipative), with beach gradients ranging from approximately 1:6 to 1:60 exposed to offshore significant wave heights of 0.5 m to 3.0 m.

The ratio of swash energy in the short-wave (f>0.05 Hz) to long-wave (f<0.05 Hz) frequency bands is found to be significantly different between the three beach types. Swash energy at short-wave frequencies is dominant on reflective and intermediate beaches and swash at long-wave frequencies is dominant on dissipative beaches; consistent with previously reported spectral signatures for the surf zone on these beach types.

The available swash spectra were classified using an automated algorithm (CLARA) into five different classes. The ordered classes represent an evolution in the spectrum shape, described by a frequency downshifting of the energy peak from the short-wave into the long-wave frequency band and an increase in the long-wave swash energy level compared to a relatively minor variation in the short-wave swash energy level. A universally common feature of spectra from all beach-states was an f^{-4} energy roll-off in the short-wave frequency band. In contrast to the broadly uniform appearance of the short-wave frequency band, the appearance of the long wave frequency band was highly variable across the beach-states.

We incorporate the results presented here and previously published observations into the morphodynamic beach-state model, and propose an ordered sequence of swash spectra under increasing and decreasing incident wave energy level. This extension of the beach-state model to include the swash zone leads to the following propositions for morphodynamic controls on the nature of the swash spectrum. (1) The short-wave part of the swash spectrum is relatively constant in form across all beach-states (f^{-4} energy roll-off) and the energy density per unit frequency is controlled by the beach face gradient alone. (2) The spectral bandwidth of the energy roll-off varies directly with offshore wave energy level and inversely with beach face gradient (or beach-state), in a manner consistent with the non-linear wave breaking criterion. (3) The infragravity part of the swash spectrum is highly variable in form across all beach-states and the energy level is related to the offshore wave energy level and surf zone morphology.

Keywords: coastal morphodynamics, beaches, beach-state model, swash zone, wave runup, beach erosion, CLARA.

1. Introduction

Two seminal papers published in 1979 introduced the now widely recognised morphodynamic beach-state model for microtidal, high-energy beaches (Short, 1979; Wright et al., 1979). The beach-state model classified beaches according to morphology and surf zone hydrodynamics. Following earlier work by Huntley and Bowen (1975), the two end-member beach-states in the model are steeply sloped reflective beaches and gently sloped dissipative beaches. Surf zones on reflective beaches are characteristically narrow to absent, thus there is minimal dissipation of incident short-wave energy (sea and swell) by breaking so

most energy is reflected at the beach face (Huntley and Bowen, 1975). Surf zones on dissipative beaches are characteristically wide, thus most of the incident short-wave energy is dissipated by turbulent breaking and there is minimal energy reflection at the beach face in that frequency band. Incident long-waves and those generated inside the surf zone are important on dissipative beaches and their energy is almost entirely reflected on even the most gently sloped beaches (Huntley and Bowen, 1975). Short (1979) and Wright et al. (1979) added four intermediate beach-states, recognising the more complex three-dimensional morphologies that can exist.

The beach-state displayed by a given beach at a particular time largely depends on the wave energy level and the sediment size (or sediment settling velocity), which have been combined into the empirical predictive parameter $\Omega = H_b / w_s T$, where H_b is the wave breaker height, w_s is the sediment settling velocity and T is the incident wave period (Wright and Short, 1984). The beach-states in the Wright and Short model are arranged in order of increasing Ω (increasing wave steepness and/or decreasing grain size) as: reflective, low-tide terrace, transverse-bar and rip, rhythmic-bar and beach, longshore-bar and trough, and dissipative (Wright and Short, 1984). Not only can a range of modal beach-states exist along a coastline that represent localized combinations of modal incident wave conditions and sediment size, but a single beach can alter beach-state with synoptic variations in incident wave conditions or longer term changes in the size of the beach sediment (Short, 1979; Wright et al., 1979; Short, 1984). Depending on localized conditions such as sediment size, wave climate, degree of embayment and other factors limiting the range of wave breaker heights (and Ω); a given beach can display either the full-range or a subset of beach-states through time (Wright and Short, 1984).

Beaches that experience a wide range in wave breaker conditions through time change state in an ordered sequence as wave steepness or energy levels increase or decrease (Sonu, 1973; Short, 1979). This ordered behavior means that by studying a set of several different beaches that represent a range of beach-states, insight can be gained into how morphodynamic processes evolve with cycles of incident wave energy. This approach has been used previously to propose evolving patterns of surf zone hydrodynamics (Wright et al., 1979; Wright, 1982) and sediment transport (Aagaard et al., 2013) associated with storm and post-storm cycles. We adopt a similar approach here to propose how swash spectral energy distributions evolve with a beach's morphodynamic response to changing levels of incident wave energy.

The swash zone is at the landward edge of the surf zone and is where the instantaneous shoreline runs up and down the beach face in response to a variety of wave types (Hughes and Turner, 1999). Herein we define swash as the oscillations in the vertical shoreline elevation relative to the short-term mean shoreline elevation (e.g. Stockdon et al., 2006; Hughes et al., 2010). The mean shoreline elevation is determined by both the tide level and wave setup level. The swash height is defined as the vertical difference between adjacent minima and maxima in the shoreline elevation time series.

While there have been numerous previous studies of the swash zone on a wide range of beach types, there has been no previous attempt to place this knowledge into the broader context of the morphodynamic beach-state model. In this paper we present an extensive field data set of swash spectra representing the full range of beach-states from reflective through intermediate to dissipative. We use this data to further develop the beach-state model by explicitly incorporating the swash zone, and at the same time organising the existing

knowledge of swash behavior into a scheme that provides further physical insight. Specifically, we hypothesise the response of the swash spectrum to changing offshore energy levels and propose the morphodynamic controls on that evolution.

2. Theoretical background and previous field observations

2.1 General concepts

Shoreline motion on natural beaches occurs across a broad range of frequencies, driven by a variety of incident wave forms. Swash spectra are typically discussed with respect to two frequency bands that correspond to short-waves and long-waves incident at the beach face. Short-wave swash derives from locally-generated wind waves and swell (e.g., Waddell, 1976; Hughes, 1992; Holland and Puleo, 2001), whereas long-wave swash (or infragravity swash) includes leaky-mode standing waves and edge waves (e.g., Huntley, 1976; Aagaard, 1991; Holland et al., 1995; Holland and Holman, 1999). A fundamental difference between incident short-waves and surf zone long-waves is that the former usually break before reaching the beach face whereas the latter typically do not. Following the convention established over many years, the frequency chosen here to separate the short-wave and long-wave bands in the swash spectrum is 0.05 Hz (e.g. Guza and Thornton, 1982; Senechal et al., 2011). This value is universally applied for convenience. It should be noted that the precise frequency separation will vary with environmental factors, and on some beaches waves that are sub-harmonics of the incident sea and swell will fall into the short-wave frequency band on the basis of this fixed criterion.

The ratio of wave steepness to beach profile gradient is fundamental to wave breaking. The limiting condition for non-breaking waves can be determined from the non-linear shallow water theory applied to standing long-waves (Carrier and Greenspan, 1958), and is

$$\varepsilon = \frac{a_s \omega^2}{g\beta^2} \tag{1}$$

where a_s is vertical swash amplitude, ω is wave radian frequency ($2\pi f$ where f is frequency), g is gravitational acceleration and β is beach slope angle in radians (assumed here to be small enough for $\tan\beta \approx \sin\beta \approx \beta$; which is satisfied for natural beach slopes). When the value of ε equals or exceeds the critical value $\varepsilon_c = 1$ then wave breaking theoretically occurs.

Previous field measurements on dissipative beaches showed that the infragravity swash energy increased with deep water wave height while short-wave swash energy remained roughly constant, suggesting short-wave energy saturation due to wave breaking (Guza and Thornton, 1982; Holman, 1983; Aagaard, 1990a). We specifically define saturation here to mean that the swash height calculated from the shoreline elevation time series variance, or equivalently the zero-moment of the energy spectrum, remains constant in a specified frequency band under increasing incident wave energy. This requires that additional energy must be either dissipated or reflected in the surf zone, or within the swash zone itself, and does not influence the magnitude of the shoreline motion in that specified frequency band.

The theoretical model for swash proposed by Huntley et al. (1977) is a useful starting point for investigating swash data from contrasting beach-states for three reasons. First, it describes the nature of the swash spectrum, and is therefore consistent with previous work characterising beach-states on the basis of wave and current spectra in the surf zone (Wright et al., 1979; Wright, 1982). Second, the magnitude and distribution of swash spectral energy

across frequencies is predicted to depend on the beach gradient, which varies consistently with beach-state. Third, the model has been argued to be universal. The foundation of the Huntley et al. model is contained in the earlier work of Miche (1944; 1951) on monochromatic swash.

2.2 Swash in the short-wave frequency band

In the Miche (1944; 1951) model for monochromatic swash the swash amplitude is proportional to the standing wave amplitude. With increasing incident wave amplitude, the swash amplitude will also increase up to the value corresponding to the maximum possible standing wave amplitude for the given beach slope. Beyond this value the increased incident energy is hypothesized to be dissipated entirely by wave breaking. This implies swash becomes saturated with the onset of wave breaking. According to the Miche (1944; 1951) model, swash driven by monochromatic standing waves should therefore be saturated for values of $\varepsilon_c \geq 1$. To put it another way, for $\varepsilon_c \geq 1$ the swash height should be constant for a given wave period and beach slope, and independent of incident wave height.

Huntley et al. (1977) extended the monochromatic Miche model into one applicable to broad-banded swash. The extended model proposed that swash energy on natural beaches is universally saturated across the bandwidth for which wave breaking is occurring. Huntley et al. (1977) describe the saturated part of the swash spectrum by

$$E = \left[\frac{\hat{\varepsilon}_c g \beta^2}{(2\pi f)^2} \right]^2 \tag{2}$$

where E is energy density, and $\hat{\varepsilon}_c$ is the critical value of the swash similarity parameter marking the onset of wave breaking and swash saturation. Here $\hat{\varepsilon}_c$ is in dimensional form

with units of $Hz^{-½}$. Based on five spectra from natural beaches representing a factor 2 range of beach gradients from 0.065 to 0.13, Huntley et al. (1977) suggested that $\hat{\varepsilon}_c$ has a value somewhere between 2 and 3 $Hz^{-½}$.

On a natural beach Equation 2 is expected to apply across the frequency bandwidth for which combinations of a_s and ω yield $\hat{\varepsilon}_c$ values consistent with wave breaking, i.e., $\varepsilon \geq \varepsilon_c$. Huntley et al. (1977) non-dimensionalised $\hat{\varepsilon}_c$ through the product $\hat{\varepsilon}_c \sqrt{\Delta f}$ and assumed that Δf was the bandwidth over which wave breaking occurred. Based on their five available spectra they suggested $\hat{\varepsilon}_c \sqrt{\Delta f}$ was universally constant with a value of about 1.0. If it is indeed constant then the beach gradient and the roll-off (breaking) bandwidth must co-vary to maintain it so.

In support of the Huntley et al. model for natural short-wave swash, numerous field studies over the past 30 years have reported swash spectra displaying an f^{-4} energy roll off (or f^{-3}) in the short-wave frequency band (e.g., Guza and Thornton, 1982; Mizuguchi, 1984; Raubenheimer and Guza, 1996; Ruessink et al., 1998; Holland and Holman, 1999; Ruggiero et al., 2004), and Raubenheimer and Guza (1996) also showed short-wave swash energy scaling with the beach gradient to the fourth power.

2.3 Swash in the long-wave (infragravity) frequency band

Some researchers have reported swash spectra that are predominantly white in the infragravity band (Ruessink et al., 1998), whereas other have reported significant peaks at a small number of frequencies (Aagaard, 1990b). The bulk of infragravity swash energy is

generally attributed to leaky mode standing waves, and progressive and standing edge waves in the adjacent surf zone (Hughes and Turner, 1999). Reviewing measurements of surf zone infragravity energy from a range of beach types, Wright (1982) noted that standing waves with the highest frequency occurred as zero-mode sub-harmonic edge waves on reflective beaches and standing waves with the lowest frequency occurred on dissipative beaches. Intermediate frequency standing waves occurred on intermediate beach-states with pronounced bar morphology. At least some of the standing waves observed were argued to be edge waves. On those beaches where reported swash spectra were not white it seems likely that there was selective amplification of particular standing wave frequencies or edge wave modes; probably due to resonant interaction with the nearshore morphology (e.g. Kirby et al., 1981; Wright, 1982).

The energy in a shoreline elevation time series is commonly represented by the significant swash height, *S*, and can be calculated as 4 times the square root of the zero-moment of the spectrum; i.e.

$$S = 4\sqrt{\int_0^\infty E(f).df} \tag{3}$$

The significant swash heights representative of the energy in the short-wave frequency band, S_s, and long-wave or infragravity wave frequency band, S_i, are calculated using Equation 3 and applying the appropriate frequency limits on the integral.

A linear relationship between S_i and the deep water wave height, H_o, has been reported by Guza and Thornton (1982) and Raubenheimer and Guza (1996) from a dissipative beach. Other researchers working on dissipative and intermediate beach types have reported a linear relationship between the normalized infragravity swash height, S_i/H_o, and the Iribarren

Number; $I_r = \tan\beta \big/ \sqrt{H_o / L_o}$, where L_o is the deepwater wave length (e.g. Holman and Sallenger, 1985; Ruessink et al., 1998). This is equivalent to a relationship where S_i is proportional to $\sqrt{H_o}$, which Stockdon et al. (2006) also favoured. There is wide variability in the values of the intercept and gradient of the linear regression lines describing these relationships (see Figure 10 in Ruessink et al., 1998 or in Senechal et al., 2011). This variability is probably in large part due to the variability in exposure of the beaches involved to the deep water wave conditions. In contrast to the dependency of short-wave swash on beach face gradient, both Stockdon et al., (2006) and Senechal et al. (2011) found no relationship between the infragravity swash height and beach face gradient. On the other hand Ruggiero et al. (2004) found that the significant infragravity swash height was inversely related to beach gradient.

On dissipative beach types, particularly under high energy conditions, the spectral energy roll-off that is characteristic of the short-wave frequency band has been observed to extend into the long-wave band (e.g. Ruessink et al., 1998; Ruggiero et al., 2004; Senechal et al., 2011). One explanation is that the frequency bandwidth over which swash saturation occurs can extend into that part of the swash spectrum dominated by infragravity waves. Ruessink et al. (1998) noted that the f^{-4} roll-off band extended to lower infragravity frequencies as the offshore energy levels increased. Possible processes contributing to energy dissipation in the infragravity band include: (a) turbulence associated with long-wave breaking in the inner surf zone on very mild beach gradients (Battjes et al., 2004); and (b) frictional dissipation by enhanced near-bed velocities due to short-waves across a wide surf zone (Ruessink, 1998).

3. Field Sites and Methods

3.1 Field sites

This study draws from several data sets collected from the eastern seaboard of Australia and Denmark. The former is exposed to a moderate-high energy, swell-dominated wave climate and the latter a low-moderate energy, wind-wave dominated wave climate (Short and Trenaman, 1992; Aagaard et al., 2013). All the beaches studied are micro-tidal and composed predominantly of sand (ranging from very fine sand to very coarse sand). The beaches displayed varying sediment sizes and degrees of exposure to the wave climate, thus a wide range of beach types, beach face gradients, and wave conditions are represented in the data set (Table 1). Specifically, beach gradients ranged over nearly an order of magnitude from 0.017 to 0.164 and offshore significant wave heights ranged from 0.50 m to 3.01 m. The number of swash spectra collected during each experiment listed in Table 1 varied, but overall representation of the broad beach-state classes of reflective, intermediate and dissipative was sufficient for this study (36 spectra from reflective, 91 from intermediate and 60 from dissipative beaches).

3.2 Field setup

Two methodologies were used for obtaining continuous time series of shoreline elevation. The first involved a resistance-type run-up wire installed across the beach, extending from the inner surf zone to beyond the maximum run-up location (e.g., Guza and Thornton, 1982; Hughes et al., 2010). The wire was maintained at approximately 0.02-0.03 m above the bed, which required continual adjustment by an observer. This elevation is expected to provide results consistent with those from video techniques (Holland et al., 1995). The run-up wire was calibrated by shorting the wire at surveyed positions along its length. The wire resistance

was logged at 10 Hz, providing a continuous time series of the shoreline location. The beach profile and location of the wire were surveyed either at the beginning or the end of the deployment, and frequently both.

The second method involved using a portable digital video camera situated on a headland, foredune or berm, and focused on the swash zone. The real world coordinates of a cross-shore line within the field of view were determined by surveying markers placed in the swash zone. Frames from the video data were sampled at 5 Hz, rectified, a pixel intensity profile extracted along a cross-shore profile from each frame and stacked through time to make a timestack. The timestack was digitized to provide a shoreline elevation time series (e.g. Aagaard and Hulm, 1989; Power et al., 2011).

3.3 Data processing

Not all data runs from every experiment were suitable for analysis. Runs interrupted by fouling of the run-up wire, wire contacting with the beach surface or poor video imagery were discarded. The remaining data runs were divided into time series lengths of 15-minutes duration to ensure stationarity with respect to the tide. A total of 187 time series were available for analysis. The shoreline positions from the run-up wire and video imagery were converted to vertical elevations using the beach face gradient. The gradient was taken as the planar slope from the surveyed profile between the highest and lowest shoreline elevation recorded for each 15-minute data run.

To make the spectral analysis consistent across the two data acquisition methods, the video imagery time series were re-sampled to provide 10 Hz time series. All time series were

then low-pass filtered with a frequency cut-off of 0.67 Hz, detrended, and a Hanning window equal to the length of the time series applied prior to calculating the spectrum. The calculated shoreline elevation spectra were then smoothed with an 11-point filter resulting in 22 degrees of freedom and a frequency resolution of 1.11×10^{-3} Hz.

4. Results

All 187 available swash spectra are shown in Figure 1, separated according to the prevailing beach-state at the time of data collection. Generally speaking the spectra from reflective beaches were characterized by a well defined primary (most energetic) peak in the short-wave frequency band, a smaller secondary peak at its first sub-harmonic, and a broader peak in the long-wave frequency band (Figure 1a). On intermediate beaches the energy was generally more broadly distributed and the most energetic frequency occurred in either the short-wave or long-wave bands (Figure 1b). The spectra from dissipative beaches generally displayed one broad peak situated inside the long-wave band (Figure 1c). A universally common feature of spectra from all beach-states was the f^{-4} energy roll-off in the short-wave band. In contrast to the broadly uniform appearance of this band across all the beach-states, the appearance of the long-wave frequency band was highly variable.

The swash spectra shown in Figure 1 were subjected to a classification algorithm known as CLARA, which uses a Euclidean metric to decide class membership and has previously been applied to wave spectra (Hamilton, 2010). CLARA returns a silhouette coefficient that can be used to guide choice on the optimal number of classes, but inspection of the output from several trials with increasing numbers of classes is necessary to make a final choice. It also identifies a medoid object (spectrum) that is representative of the cluster properties. A

full description of the algorithm and its application to wave spectra is presented in Hamilton (2010). For the analysis performed here, all the swash spectra were normalized to the energy level at the peak frequency in order to avoid classification based on overall spectral energy; the shape of the spectrum is what we were seeking to classify.

The available spectra were classified into three classes that broadly corresponded to reflective, intermediate and dissipative beach-states. The optimal number of classes for our data set, however, was five. In the context of the beach-state model it would be conceptually convenient to consider only three classes, however, it is instructive for later discussion to explore the five classes: a reflective class, low-energy and high-energy intermediate classes, and two dissipative classes. The medoids for each class are shown individually in Figure 2 as well as overlaid collectively on a single plot. The number of spectra in each of Classes 1 to 5 was 45, 46, 41, 34, and 21, respectively. The general properties of Class 1 (and possibly Class 2) are broadly consistent with those previously described for swash spectra from reflective beaches (cf. Figure 2a and 2b with Figure 1a). Classes 4 and 5 are broadly consistent with the previous description of swash spectra from dissipative beaches (cf. Figure 2d and 2e with Figure 1c). Finally, Classes 2 and 3 are also broadly consistent with the properties previously described for swash spectra from intermediate beaches (cf. Figure 2b and 2c with Figure 1b). It is important to note, however, that membership in any of the 5 classes was not uniquely associated with a single beach-state. Classes 1 to 4 represent an evolution in the spectrum shape described by a frequency downshifting of the energy peak from the short-wave into the long-wave band and an increase in the infragravity swash energy level compared to a consistent short-wave swash energy level. Class 5 contains characteristics of dissipative beaches, but with the energy level of the f^{-4} roll-off band being considerably smaller than all other spectra.

The ratio of short-wave swash energy, E_s, to infragravity swash energy, E_i, is shown in Figure 3 for each beach-state as a box-and-whisker plot. The vertical extent of the box represents the interquartile range of observations for each beach-state and the horizontal line across the box represents the median value. The dashed lines above and below the box shows the extent of the rest of the data. The red crosses show outliers. The notch in the box represents the 95 % confidence interval for the median. The distribution of the E_s/E_i values from each beach-state was skewed with the longer tail towards larger values. Part of the reason for the overly long tail for the reflective beaches was that significant sub-harmonic energy was included in the short-wave band due to the application of a fixed demarcation frequency between short-waves and long-waves of 0.05 Hz (Section 2.1). The median E_s/E_i value for the reflective, intermediate and dissipative beach-states was 2.71, 1.81 and 0.52, respectively. The median E_s/E_i value for the reflective and intermediate beach-states was significantly greater than the value for the dissipative beach-state at the 95% confidence level. The median E_s/E_i value for the reflective beach-state was also significantly greater than the value for the intermediate beach-state, but only at the 90% confidence level. All of the spectra from reflective beaches and more than 75% of the spectra from intermediate beaches had a total swash energy level in the short-wave frequency band larger than that in the infragravity band (i.e. E_s/E_i >1). For 95% of the spectra from dissipative beaches the converse was true; the total infragravity swash energy was greater than the short-wave swash energy (i.e. E_s/E_i <1).

A universally common feature of spectra from all beach-states was the energy roll-off in the short-wave band. The bandwidth of the f^{-4} roll-off was smallest on reflective beaches,

with the lowest frequency to which the f^{-4} roll-off extended being much greater than 0.05 Hz (Figure 1a). The bandwidth of the f^{-4} roll-off was largest on dissipative beaches and extended well into the infragravity band (Figure 1c). On intermediate beaches the bandwidth of the f^{-4} roll-off was intermediate of the reflective and dissipative situations; and while the lowest frequency to which the roll-off extended was smaller than on reflective beaches, it generally sat within the short-wave frequency band (Figure 1c).

The lowest frequency to which the f^{-4} roll-off band extended, f_s, was determined for each spectrum in the following way. The best fit linear regression line (and 95% confidence interval) was fitted to that part of the spectrum displaying an f^{-4} energy roll-off. This line was extended in the down-frequency direction, and the value of f_s was taken as the frequency at which the spectrum departed significantly from the regression line (see also Ruessink et al., 1998). Investigation showed that f_s was highly positively correlated with the beach gradient (r^2= 0.71 and p=0.000) and the significant short-wave swash height, S_s (r^2=0.62 and p=0.000), and weakly correlated with the overall significant swash height, S (r^2=0.25 and p=0.0006), and the infragravity swash height, S_i (r^2=-0.18 and p=0.015). While a re-arranged form of Equation 1 might seem a reasonable parameter to scale against f_s the presence of beach gradient in the denominator is problematic. The values of f_s are therefore scaled against $\beta\sqrt{gS_s}/S_i$ in Figure 4. The gravitational acceleration and the significant infragravity swash height are included only to be dimensionally correct. The least squares regression line fitted to the data is given by

$$f_s = 0.0834 + 0.0400\log\left(\frac{\beta\sqrt{gS_s}}{S_i}\right) \tag{4}$$

with an r^2= 0.65 (p=0.000) which is significant at the 95% confidence level.

The Huntley et al. (1977) model for short-wave swash spectra, Equation 2, can be re-written in a simpler form as

$$E = \alpha f^{-4} \tag{5}$$

where the proportionality coefficient α is

$$\alpha = \frac{\hat{\varepsilon}_c^2 g^2 \beta^4}{(2\pi)^4} \tag{6}$$

Re-expressing Equation 6 as

$$\sqrt{\alpha} = \hat{\varepsilon}_c \sqrt{\frac{g^2 \beta^4}{2\pi^4}} \tag{7}$$

shows that the slope of the linear regression line between measured values of $\sqrt{\alpha}$ and $\sqrt{g^2 \beta^4 (2\pi)^{-4}}$ will yield a value for $\hat{\varepsilon}_c$. A value of α was obtained for each available spectrum as the slope of the linear regression line between E and f^{-4} (viz., Equation 5) over a common frequency range that was inside the roll-off band for all the spectra (i.e., 0.15–0.25 Hz). A histogram of the r^2-values for these regression lines is shown in Figure 5a. Most had a value greater than 0.8, only three were less than 0.5 and only one was not significant at the 95 % confidence level. The value of $\sqrt{\alpha}$ for each spectrum is shown in Figure 5b as a function of $\sqrt{g^2 \beta^4 (2\pi)^{-4}}$. While considerable scatter exists in the data, it does appear that the swash energy level in the f^{-4} roll-off band does scale with β^4. Given the high power, some of the scatter may relate to the precision with which the beach gradient can be estimated. The linear regression line fitted to all the data has an associated r^2=0.68 (p=0.000), which is significant at the 95 % confidence level, and the slope of the regression line yields a value of $\hat{\varepsilon}_c = 2.75 \pm 0.22$ Hz$^{-½}$. It could be argued that the trend in those data from dissipative beaches

is constant (Figure 5b), but ignoring this data has a minimal impact on the estimated value of $\hat{\varepsilon}_c$ (viz. $\hat{\varepsilon}_c = 2.76 \pm 0.26$).

Individual estimates of the non-dimensional form of $\hat{\varepsilon}_c$ for each available spectrum, $\hat{\varepsilon}_c\sqrt{\Delta f}$, are plotted against beach gradient in Figure 6. The lower boundary of the f^{-4} roll-off band was estimated by our previously described values of f_s (Figure 4) and the upper boundary was taken as the high frequency limit of our spectra. The value of Δf was therefore calculated as 0.5-f_s. Consistent with model expectations the values of $\hat{\varepsilon}_c\sqrt{\Delta f}$ are approximately constant for most of the data set. Only for two deployments during dissipative beach conditions was there large departure from the constant value. Spectra from those two deployments showed unusually small f_s values and thus large Δf values. Excluding the data from these two deployments, the mean value of $\hat{\varepsilon}_c\sqrt{\Delta f}$ (with 95 % confidence interval) was 2.25 ± 1.72.

The beaches represented in our data set display a wide range of exposure to offshore wave energy; ranging from long open coast beaches through to embayed pocket beaches, including one beach at the landward limit of a large bay. There is a large amount of variation in the swash energy between the beaches for any given offshore wave condition. Furthermore, for any single deployment the variation in offshore wave conditions was generally small. Our data set is therefore not useful for investigating the relationship between the infragravity swash energy and offshore wave conditions. We did investigate the dependency of the significant infragravity swash height on beach gradient and, in contrast to the case of short-wave swash energy (Figure 5), infragravity swash energy was independent of beach gradient (Figure 7).

5. Discussion

The 187 swash spectra studied here were obtained from multiple, dynamically diverse sets of beach conditions; 9 different beaches over 36 different deployments. Beach gradients spanned the range 0.017 to 0.164; indicative of fine through to coarse sandy beaches. Offshore wave heights spanned 0.55 m to >3.00 m; indicative of both fair-weather and storm conditions. Beach-states represented in the data set include the 3 broad types; steeply-sloped reflective, moderately-sloped intermediate and gently-sloped dissipative.

The Huntley et al. swash model predicts that the swash energy density per unit frequency in the wave breaking band is dependent on the maximum possible standing wave amplitude for each frequency in that bandwidth, and is therefore dependent only on the beach gradient. The beach gradient and frequency bandwidth for wave breaking are expected to co-vary in a manner consistent with that implicit in the wave breaking criterion (Equation 1) in order to maintain energy saturation. For example, increased offshore wave energy often results in increased wave steepness, offshore sediment transport and a reduction in beach gradient (e.g. Komar, 1998). The gentler beach gradient and shallower water depths offshore mean that larger and longer period waves will break, thus the bandwidth over which wave breaking occurs expands to lower frequencies. Accepting the premise of Huntley et al. (1977) that the width of the f^{-4} roll-off band in swash spectra corresponds to the bandwidth for which waves are breaking in the surf zone, in effect means that the value of $\hat{\varepsilon}_c \sqrt{\Delta f}$ is universally constant.

Three key elements of the Huntley et al. swash model are supported by the data presented here: (i) the ubiquitous presence of an f^{-4} roll-off band (Figure 1); (ii) the dependence of the short-wave swash energy on the beach gradient to the fourth power (Figure 5); and (iii) the bandwidth of the f^{-4} roll-off varying inversely with beach gradient (Figure 4). The extensive data set analysed in this study provided an estimate for $\hat{\varepsilon}_c$ of 2.75 ± 0.22 Hz$^{-½}$, which compares well with the range of 2 to 3 suggested by the much smaller data set of Huntley et al. (1977). Furthermore, across most of our data set the value of $\hat{\varepsilon}_c \sqrt{\Delta f}$ was universally constant. The only exceptions were spectra from deployments on two dissipative beaches where the f^{-4} roll-off extended deep into the long-wave frequency band. Excluding these exceptions, the constant value for $\hat{\varepsilon}_c \sqrt{\Delta f}$ (with 95 % confidence interval) from our data set was 2.25 ± 1.72, which is a little more than twice the value of unity suggested by Huntley et al. (1977). The method used here and by Ruessink et al. (1998) to determine the roll-off bandwidth differed to that used by Huntley et al. (1977). The latter compared the offshore wave spectrum to the swash spectrum to infer the bandwidth over which wave breaking occurred. We determined the lowest frequency at which the spectrum significantly departed from an f^{-4} roll-off, which could result in a larger estimate of Δf and hence $\hat{\varepsilon}_c \sqrt{\Delta f}$.

The unusually large values of $\hat{\varepsilon}_c \sqrt{\Delta f}$ observed during two of our deployments on dissipative beaches suggest that the Huntley et al. swash model is invalid when the f^{-4} roll-off band extends deep into the infragravity frequency band. This is further confirmed by results from a high energy dissipative beach presented by Ruggiero et al. (2004). Their data set contained swash spectra collected from several locations alongshore (displaying variable

beach gradient) under constant offshore wave conditions. Over a range of beach gradients from 0.005 to 0.025 they found that $\hat{\varepsilon}_c\sqrt{\Delta f}$ was not constant, rather it was a function of beach gradient. It is perhaps unsurprising that the model breaks down on some dissipative beaches; a model premise is that the f^{-4} roll-off band corresponds to the bandwidth over which waves are breaking, and this is unlikely to be the case for low frequency infragravity waves. It is surprising however, that an f^{-4} roll-off commonly extends into the long-wave band on dissipative beaches (Figure 1c; Ruessink et al. 1998; Ruggiero et al., 2004). Several studies have shown that shoreline motion driven by both short-waves and long-waves is nearly-parabolic in time, appearing as consecutive truncated parabolas (e.g., Hughes, 1992; Puleo et al., 2000; Ruggiero et al., 2004). Mase (1988) demonstrated that the spectrum of a single parabola displays an f^{-4} roll-off, which might provide a partial explanation.

There is considerable data scatter in Figure 6, even in the region where the value of $\hat{\varepsilon}_c\sqrt{\Delta f}$ is approximately constant. Some of this is experimental error, but it is likely that unaccounted factors contribute to the scatter. It might be that Equation 1 does not correctly describe the onset of wave breaking. This would mean that the amount of 'excess' energy dissipation in the surf zone assumed in the Huntley et al. swash model is incorrect. The laboratory data of Guza and Bowen (1976) suggest monochromatic waves saturate for values of $\varepsilon_c = 3$ rather than 1. A similar result has not been established for broad-banded swash, but there is certainly a wide range in the wave-height-to-water-depth ratios of depth-limited waves observed in the inner surf zone of natural beaches (e.g. Thornton and Guza, 1982; Wright et al., 1982; Sallenger and Holman, 1985). The beach face gradient, measured as the gradient between the maximum and minimum shoreline elevation, also may not be the ideal measure in all cases. Longer period waves in particular will likely experience energy

reflection from the inner surf zone slope as well as the beach face. Furthermore, Baldock et al. (1998) and Bryan and Coco (2010) describe low frequency swash energy unrelated to incident waves in the corresponding frequency band.

There are clear qualitative differences in the shape of the mean swash spectrum from each beach type, however, there is a large range in the swash spectra within each beach type; particularly for intermediate beaches (Figure 1). On reflective and intermediate beach-states there was more swash energy in the short-wave than the long-wave band, whereas on the dissipative beach-state there was more energy in the long-wave band (Figure 3). Unsupervised classification of the spectra yielded five classes. There is qualitative similarity between the medoid spectra from Classes 1 and 2 and the mean spectrum for the reflective beach-state, and similarly with Classes 2 and 3 with the intermediate beach-state and Classes 3 and 4 with the dissipative beach-state. The fifth spectral class appears to be related to dissipative conditions with unsaturated swash. The principal differences between the classes were the width of the f^{-4} energy roll-off band and the relative amount of energy in the infragravity swash band.

Class memberships did not correspond uniquely to individual beach-states, most likely because much of the data was not collected under equilibrium conditions. The response time of morphology is much greater than the variation in hydrodynamic forcing so in order for the beach-state to be in equilibrium the wave conditions must be constant for up to several weeks (e.g. Wright et al., 1984; 1985; Short, 1987; Ranasinghe et al., 2004). Many features of the swash spectra did vary with beach face gradient, which is a broad (and less restrictive) proxy for beach-state (Table 1; Wright et al., 1979; Short, 1979), including the width of the f^{-4} energy roll-off band (Figure 5).

Previous studies have synthesized observations from different beach-states into the morphodynamic beach-state model to propose evolving patterns of surf zone hydrodynamics (Wright et al., 1979; Wright, 1982) and sediment transport (Aagaard et al., 2013) associated with storm and post-storm cycles. We adopt a similar approach here to propose how swash behavior (represented by the swash spectrum) evolves with a beach's morphodynamic response to changing offshore wave conditions. Figure 8 shows an idealized evolutionary sequence of swash spectra under rising energy conditions; which is underpinned by the spectral classes identified here, the Huntley et al. swash model, and other observations of short-wave and infragravity swash behavior reported here and elsewhere. The beach-states showing idealised surf zone morphology and relative beach face gradients are also depicted.

In Figure 8a the grey spectrum is the initial condition and shows the general characteristics for the reflective beach-state in equilibrium: a more energetic short-wave rather than infragravity swash band; a well-defined short-wave swash energy peak; and a peak at the first sub-harmonic, probably related to sub-harmonic standing edge waves (e.g. Wright, 1982; Guza and Inman, 1975). With an increase in offshore energy level the black spectrum in Figure 8a is expected to develop; similar characteristics to the preceding spectrum but with increased incident and sub-harmonic energy levels (e.g. Wright, 1980). The energy density in the roll-off band remains constant, consistent with the Huntley et al. swash model, but here we have shown the roll-off bandwidth extending to lower frequencies to demonstrate one possible disequilibrium condition in which the value of $\hat{\varepsilon}_c\sqrt{\Delta f}$ departs from a constant value.

With increasing offshore wave energy level the value of Ω will cross a threshold and there will be a change in beach-state to intermediate surf zone morphologies and beach face gradients (Wright and Short, 1984). The black spectrum in Figure 8b is one broadly representative of lower energy intermediate beach-states (low-tide terrace, transverse-bar and rip or rhythmic-bar and beach). The grey spectrum is the same as the black spectrum in Figure 8a for comparison. The total short-wave swash energy is still larger than the infragravity swash energy, although the latter has increased. For low energy intermediate beach-states with accentuated surf zone morphology we expect a peaky structure in the infragravity swash band due to preferential amplification of edge wave modes or shore-normal surf beat by shallow bars (e.g. Wright, 1982; Symonds and Bowen, 1984). The energy density in the roll-off band is reduced and the roll-off bandwidth increased due to the reduction in beach face gradient, consistent with the Huntley et al. swash model.

Continuing to increase the offshore wave energy level will cause the beach to continue transitioning through the intermediate beach-states as threshold values of Ω are exceeded. The black spectrum in Figure 8c is one broadly representative of higher energy intermediate beach-states (rhythmic-bar and beach or longshore-bar and trough). The grey spectrum is the same as the black spectrum in Figure 8b for comparison. The energy density in the infragravity swash band has continued to increase and the total infragravity swash energy is now comparable to the total short-wave swash energy. The infragravity swash band is now featureless, consistent with the surf zone morphology becoming more subdued with no preferential amplification of resonant frequencies (e.g. Kirby et al., 1981; Wright, 1982). The energy density in the short-wave roll-off band has decreased and the width of the roll-off band has increased, consistent with the decrease in beach face gradient.

If the offshore wave energy level continues to increase and Ω exceeds 6 then the beach-state will change to dissipative. The black spectrum in Figure 8d is one broadly representative of high energy dissipative beaches. The grey spectrum is the same as the black spectrum in Figure 8c for comparison. The total infragravity swash energy now exceeds the short-wave swash energy. The infragravity swash band remains largely featureless and the roll-off band extends well into infragravity frequencies (e.g. Ruessink et al., 1998; Ruggiero et al., 2004; Senechal et al., 2011). The energy density in the roll-off band has decreased, consistent with the decrease in beach gradient, but may not be quantitatively consistent with the Huntley et al. swash model, which appears to break down in the case of high energy dissipative conditions (Figure 6).

The evolutionary sequence of swash spectra just described under increasing offshore wave conditions may occur in full or in part. If the beach starts in any of the higher level beach-states or the increasing energy event is of insufficient duration then only a section of the sequence will occur. The beach-state response will lag the increase in offshore energy, as will the reduction of beach face gradient. Therefore the energy density in the roll-off band will be greater than expected based on the Huntley et al. model. The evolutionary sequence of swash spectra under decreasing offshore wave energy level is generally expected to be the reverse of the sequence just described, except that any disequilibrium due to morphological lags will result in less than expected energy density levels in the roll-off band.

6. Conclusions

The beach-states, reflective through intermediate to dissipative, represent a continuum of decreasing beach face gradient. Many characteristics of swash behavior described here were

demonstrated to be directly related to the beach-state or indirectly so through a relationship with beach gradient. The occasional lack of clear connection to beach-state was most likely due to disequilibrium between the beach-state (classified largely according to the surf zone morphology), the beach face gradient and the offshore wave conditions during the field deployments.

The relative energy levels of short-wave swash and infragravity swash were different between beach-states, with the former (latter) becoming less (more) important with a change from the reflective through to the dissipative beach-state. The short-wave swash energy was largely independent of deep water wave conditions and highly dependent on the beach gradient to the fourth power. The converse was true for the infragravity swash energy. The spectral character of the infragravity swash band was highly variable whereas the character of the short-wave swash band was broadly consistent across all beach-states. Specifically, the short-wave swash band was dominated by an f^{-4} energy roll-off. The bandwidth of this roll-off varied inversely with beach gradient. The Huntley et al. model for swash behavior in the short-wave band, specifically for the bandwidth over which wave breaking occurs, was broadly supported by the data presented here. Further work is required to understand the extension of the f^{-4} energy roll-off into the infragravity wave band; since notwithstanding the presence of an f^{-4} energy roll-off the model appears to become invalid ($\hat{\varepsilon}_c\sqrt{\Delta f}$ does not remain constant) for particular dissipative beach conditions.

The general observations of swash behavior presented here and elsewhere have been integrated into the beach-state model and an evolutionary sequence of swash spectra has been hypothesised under increasing and decreasing offshore wave energy conditions. This extension of the beach-state model to include the swash zone leads to the following

propositions for morphodynamic controls on the nature of the swash spectrum. (1) The short-wave part of the swash spectrum is relatively constant in form across all beach-states (f^{-4} energy roll-off) and the energy density per unit frequency is controlled by the beach face gradient alone. (2) The spectral bandwidth of the energy roll-off varies directly with offshore wave energy level and inversely with beach face gradient (or beach-state), in a manner consistent with the non-linear wave breaking criterion. (3) The infragravity part of the swash spectrum is highly variable in form across all beach-states and the energy level is related to the offshore wave energy level and surf zone morphology. White infragravity swash spectra are probably related to high incident wave energy conditions and/or subdued morphology in the surf zone (dissipative and longshore-bar and trough beach-states), whereas non-white infragravity swash spectra are probably related to moderate-low incident wave energy conditions and/or accentuated surf zone morphology (longshore-bar and trough and rhythmic-bar and beach beach-states) resulting in preferential excitation of particular standing wave frequencies or edge wave modes.

Further work is required to establish the efficacy of the proposed swash component of the beach-state model. This can probably only be achieved with video-acquired measurements of swash spectra, beach gradient, and classified beach-state, together with offshore wave conditions. Long term video measurements (at appropriate data capture rates) made on a modally intermediate beach that displays the full range of beach-states in response to the available range of incident wave conditions would be ideal.

Acknowledgments

The Australian Research Council funded many of the experiments reported here. Colleagues who provided valuable assistance with these experiments at various times include, Andrew Aouad, Nick Cartwright, Aaron Coutts-Smith, David Hanslow, David Mitchell, Adrienne Moseley, Peter Nielsen, Tony Peric, and Felicia Weir. The Danish experiments were funded by the Danish Natural Sciences Research Council.

References

Aagaard, T., 1990a. Swash Oscillations on Dissipative Beaches - Implications for Beach Erosion. Journal of Coastal Research SI9, 738-752.

Aagaard, T., 1990b. Infragravity waves and nearshore bars in protected, storm dominated coastal environments. Marine Geology 94, 181-203.

Aagaard, T., 1991. Multiple-bar morphodynamics and its relation to low-frequency edge waves. Journal of Coastal Research 7, 801-813.

Aagaard, T., Hulm, J. 1989. Digitisation of wave runup using video records. Journal of Coastal Research 5, 547-551.

Aagaard, T., Greenwood, B., Hughes, M.G., 2013. Sediment transport on dissipative, intermediate and reflective beaches. Earth-Science Reviews 124, 32-50.

Baldock, T.E., Holmes, P., Bunker, S., van Weert, P., 1998. Cross-shore hydrodynamics within an unsaturated surf zone. Coastal Engineering 34, 173-196.

Battjes, J.A., Bakkenes, H.J., Janssen, T.T., van Dongeren, A.R., 2004. Shoaling of sub-harmonic gravity waves. Journal of Geophysical Research 109, C02009, doi: 10.1029/2003JC001863.

Bryan, K.R., Coco, G., 2010. Observations of non-linear runup patterns on plane and rhythmic beach morphology. Journal of Geophysical Research 115, C09017, doi: 10.1029/2009JC005721.

Carrier, G.F., Greenspan, H.P., 1958. Water waves of finite amplitude on a sloping beach. Journal of Fluid Mechanics 4, 97-109.

Guza, R.T., Inman, D.L., 1975. Edge waves and beach cusps. Journal of Geophysical Research 80, 2997-3012.

Guza, R.T., Bowen, A.J., 1976. Resonant interaction for waves breaking on a beach. Proceedings 15th International Coastal Engineering Conference, ASCE, New York, 560-579.

Guza, R.T., Thornton, E.B., 1982. Swash oscillations on a natural beach. Journal of Geophysical Research 87, 483-491.

Hamilton, L.J., 2010. Characterising spectral sea wave conditions with statistical clustering of actual spectra. Applied Ocean Research 32, 332-342.

Holland, K.T., Holman, R.A., 1999. Wavenumber-frequency structure of infragravity swash motions. Journal of Geophysical Research 104, 13479-13488.

Holland, K.T., Puleo, J.A., 2001. Variable swash motions associated with foreshore profile change. Journal of Geophysical Research 106, 4613-4623.

Holland, K.T., Raubenheimer, B., Guza, R.T., Holman, R.A., 1995. Run-up kinematics on a natural beach. Journal of Geophysical Research 100, 4985-4993.

Holman, R.A., 1983. Edge waves and the configuration of the shoreline, in: Komar, P.D., (Ed.), CRC Handbook of Coastal Processes and Erosion. CRC Press Inc., Boca Raton, Florida, pp. 21-33.

Holman, R.A., Sallenger Jr., A.H., 1985. Setup and swash on a natural beach. Journal of Geophysical Research 90, 945-953.

Hughes, M.G., 1992. Application of a non-linear shallow water theory to swash following bore collapse on a sandy beach. Journal of Coastal Research 8, 562-578.

Hughes, M.G., Turner, I.L., 1999. The beach face, in: Short, A.D. (Ed.), Handbook of Beach and Shoreface Morphodynamics. Wiley, pp. 119-144.

Hughes, M.G., Moseley, A.S., Baldock, T.E., 2010. Probability distributions for wave runup on beaches. Coastal Engineering 57, 575-584

Huntley, D.A., 1976. Long-period waves on a natural beach. Journal of Geophysical Research 81, 6441-6450.

Huntley, D.A., Bowen, A.J., 1975. Comparison of the hydrodynamics of steep and shallow beaches, in: Hails, J., Carr, A. (Eds.), Nearshore Sediment Dynamics and Sedimentation. Wiley, Ch. 4.

Huntley, D.A., Guza, R.T., Bowen, A.J., 1977. A universal form for shoreline run-up spectra? Journal of Geophysical Research 82, 2577-2581.

Kirby, J.T., Dalrymple, R.A., Liu, P.L.F., 1981. Modification of edge waves by barred-beach topography. Coastal Engineering 5, 35-49.

Komar, P.D., 1998. Beach processes and sedimentation. Prentice Hall, New Jersey, 544 pp.

Mase, H., 1988. Spectral characteristics of random wave run-up. Coastal Engineering 12, 175-189.

Miche, R., 1944. Mouvement ondulatoires de mers en profondeur constante ou decroissante. Ann. Ponts Chaussees 114, 25-78.

Miche, R., 1951. Le pouvoir reflechissant des ouvrages maritimes exposes a l'action de la houle. An. Ponts Chaussees 121, 285-319.

Mizuguchi, M., 1984. Swash on a natural beach. 19th International Conference on Coastal Engineering, ASCE, Houston, Texas.

Power, H.E., Holman, R.A., Baldock, T.E., 2011. Swash zone boundary conditions derived from optical remote sensing of swash zone flow patterns. Journal of Geophysical Research 116, doi:10.1029/2010JC006724.

Puleo, J.A., Beach, R.A., Holman, R.A., Allen, J.S., 2000. Swash zone sediment suspension and transport and the importance of bore-generated turbulence. Journal of Geophysical Research 105, 17021-17044.

Ranasinghe, R., Symonds, G., Black, K., Holman, R.A., 2004. Morphodynamics of intermediate beaches: a video imaging and numerical modeling study. Coastal Engineering 51, 629-655.

Raubenheimer, B., Guza, R.T., 1996. Observations and predictions of run-up. Journal of Geophysical Research 101, 25575-25587.

Ruessink, B.K., 1998. Bound and free infragravity waves in the nearshore zone under breaking and non-breaking conditions. Journal of Geophysical Research 103, 12795-12805.

Ruessink, B.K., Kleinhans, M.G., van den Beukel, P.G.L., 1998. Observations of swash under highly dissipative conditions. Journal of Geophysical Research 103, 3111-3118.

Ruggiero, P., Holman, R.A., Beach, R.A., 2004. Wave run-up on a high-energy dissipative beach. Journal of Geophysical Research 109, C06025, doi:10.1029/2003JC002160.

Sallenger, A.H., Holman, R.A., 1985. Wave energy saturation on a natural beach of variable slope. Journal of Geophysical Research 90, 11939-11944.

Senechal, N., Coco, G., Bryan, K.R., Holman, R.A., 2011. Wave runup during extreme storm conditions. Journal of Geophysical Research 116, C07032, doi:10.1029/2010JC006819.

Short, A.D., 1979. Three dimensional beach-stage model. Journal of Geology 87, 553-571.

Short, A.D., 1984. Temporal change in beach type resulting from a change in grain size. Search 15, 228-230.

Short, A.D., 1987. A note on the controls of beach type and change, with S.E. Australian examples. Journal of Coastal Research 3, 387-395.

Short, A.D., Trenaman, N.L., 1992. Wave climate of the Sydney region: an energetic and highly variable ocean wave regime. Australian Journal of Marine and Freshwater Research 43, 765-791.

Sonu, C.J., 1973. Three-dimensional beach changes. Journal of Geology 81, 42-64.

Stockdon, H.F., Holman, R.A., Howd, P.A., Sallenger Jr., A.H. 2006. Empirical parameterization of setup, swash, and run-up. Coastal Engineering 53, 573-588.

Symonds, G., Bowen, A.J., 1984. Interaction of nearshore bars with incoming wave groups. Journal of Geophysical Research 89, 1953-1959.

Thornton, E.B., Guza, R.T., 1982. Energy saturation and phase speeds measured on a natural beach. Journal of Geophysical Research 87, 9499-9508.

Waddell, E., 1976. Swash-groundwater-beach profile interactions, in: Davis Jr., R.A., Ethington, R.L. (Eds.), Beach and Nearshore Sedimentation. Society of Economic Paleontologists and Mineralogists, pp. 115-125.

Wright, L.D., 1980. Beach cut in relation to surf zone morphodynamics. International Conference on Coastal Engineering, Sydney, 978-996.

Wright, L.D., 1982. Field observations of long period surf zone standing waves in relation to contrasting beach morphologies. Australian Journal of Marine and Freshwater Research 33, 181-201.

Wright, L.D., Short, A.D., 1984. Morphodynamic variability of surf zones and beaches; a synthesis. Marine Geology 56, 93-118.

Wright, L.D., Chappell, J., Thom, B.G., Bradshaw, M.P., Cowell, P.J., 1979. Morphodynamics of reflective and dissipative beach and inshore systems, southeastern Australia. Marine Geology 32, 105-140.

Wright, L.D., Guza, R.T., Short, A.D., 1982. Dynamics of a high-energy dissipative surf zone. Marine Geology 45, 41-62.

Wright, L.D., May, S.K., Short, A.D., Green, M.O., 1984. Beach and surf zone equilibria and response times. 19th International Conference on Coastal Engineering, ASCE, Houston, 2150-2164.

Wright, L.D., Short, A.D., Green, M.O., 1985. Short term changes in the morphodynamic states of beaches and surf zones: an empirical predictive model. Marine Geology 62, 339-364.

Table 1
Summary of experimental conditions during each deployment: method refers to the use of a resistance-type runup wire or video technique, Type refers to the beach type (R is reflective, TBR is transverse-bar and rip, RBB is rhythmic-bar and beach, LBT is longshore-bar and trough, D is dissipative), β is beach gradient in the active swash zone, and H is the measured deep water significant wave height or the estimated breaker height in the outer surf zone.

Site	Date	Method	Type	β	H (m)
Avoca Beach	14.10.2003	wire	LBT	0.121	1.77
Avoca Beach	16.11.2004	wire	LBT	0.072	1.56
Avoca Beach	17.11.2004	wire	LBT	0.082	1.01
The Spit	11.03.2009	video	D	0.080	3.01
The Spit	12.03.2009	video	D	0.082	2.34
Moreton Island	06.12.2004	wire	D	0.048	1.76
Narrabeen Beach (line 1a)	01.06.1988	video	TBR	0.135	1.17
Narrabeen Beach (line 2a)	01.06.1988	video	TBR	0.164	1.17
Narrabeen Beach (line 1b)	01.06.1988	video	TBR	0.100	1.17
Narrabeen Beach (line 2b)	01.06.1988	video	TBR	0.123	1.17
Pearl Beach (line 1a)	05.05.1988	video	R	0.105	1.22
Pearl Beach (line 2a)	05.05.1988	video	R	0.152	1.22
Pearl Beach (line 1b)	05.05.1988	video	R	0.090	1.22
Pearl Beach (line 2b)	05.05.1988	video	R	0.102	1.22
Pearl Beach (line 1)	26.03.1998	wire	R	0.108	2.05
Pearl Beach (line 2)	26.03.1998	wire	R	0.098	2.05
Seven Mile Beach	21.05.1988	video	D	0.035	1.84
Seven Mile Beach (line 1a)	22.05.1988	video	D	0.030	2.33
Seven Mile Beach (line 2a)	22.05.1988	video	D	0.025	2.33
Seven Mile Beach (line 1b)	22.05.1988	video	D	0.027	2.33
Seven Mile Beach (line 2b)	22.05.1988	video	D	0.020	2.33
Seven Mile Beach	21.07.2004	wire	D	0.030	1.78
Seven Mile Beach	22.07.2004	wire	D	0.031	1.65
Skallingen	17.03.1991	video	D	0.020	0.55
Skallingen	19.03.1991	video	D	0.017	1.88
Skallingen	20.03.1991	video	D	0.019	1.06
Staengehus Beach	11.09.1987	video	RBB	0.105	1.10†
Staengehus Beach (line 1)	15.09.1987	video	RBB	0.105	1.80†
Staengehus Beach (line 2)	15.09.1987	video	RBB	0.114	1.80†
Staengehus Beach (line 1)	30.11.1987	video	D	0.087	3.00†
Staengehus Beach (line 2)	30.11.1987	video	D	0.105	3.00†
Staengehus Beach (line 1)	17.11.1990	video	RBB	0.114	1.80†
Staengehus Beach (line 2)	17.11.1990	video	RBB	0.061	1.80†
Staengehus Beach (line 1)	18.11.1990	video	RBB	0.105	0.85†
Staengehus Beach (line 2)	18.11.1990	video	RBB	0.096	0.85†
Stradbroke Island	06.11.2001	wire	LBT	0.038	0.85

† Estimated breaker height in the outer surf zone

Figure captions

Figure 1. Swash energy spectra from (a) reflective, (b) intermediate, and (c) dissipative beach-states. The grey lines show individual spectra, the coloured lines show the average spectrum for the beach-state, the black line represents an f^{-4} energy roll-off and the vertical dashed line demarcates the short-wave and long-wave frequency bands.

Figure 2. Medoids of spectral Classes 1 to 5 are shown in (a) to (e), respectively and the same spectra are re-plotted together in (f).

Figure 3. Box and whisker plot of the energy ratios E_s/E_i measured from each beach-state. See text for explanation of the statistical parameters represented.

Figure 4. The lowest frequency to which the f^{-4} roll-off band extends plotted as a function of beach gradient and normalised significant short-wave swash height. The symbols identify beach-states: reflective (red squares), intermediate (green circles) and dissipative (blue triangles). The line represents the linear least-squares regression model for the data.

Figure 5. (a) Frequency histogram of r^2-values obtained when fitting a straight line with a fixed slope of f^{-4} to each spectrum in the data set. (b) Scatter plot of the data used to estimate $\hat{\varepsilon}_c$ in Equation 7. Values on the axes are explained in the text. The symbols identify beach-states: reflective (red squares), intermediate (green circles) and dissipative (blue triangles). The solid line represents the linear least-squares regression model fitted to all the data.

Figure 6. The universal constant, $\hat{\varepsilon}_c\sqrt{\Delta f}$, from the Huntley et al. (1977) model for swash plotted against beach gradient. The symbols identify beach-states: reflective (red squares), intermediate (green circles) and dissipative (blue triangles). The horizontal line shows $\hat{\varepsilon}_c\sqrt{\Delta f} = 2.25$.

Figure 7. The significant infragravity swash height plotted against beach gradient. The symbols identify beach-states: reflective (red squares), intermediate (green circles) and dissipative (blue triangles).

Figure 8. Schematic diagram integrating the general features of swash behavior into the Wright and Short (1984) morphodynamic beach-state model. The idealised spectra on the left hand side are representative of beach-states under increasing energy conditions: (a) reflective, (b) low-energy intermediate, (c) high-energy intermediate and (d) dissipative beach-states. See text for further explanation. The vertical dashed line shows the demarcation between the short-wave and long-wave frequency bands. The circles show the low frequency boundary of the roll-off band. The right hand side is an idealized representation of the surf zone morphology and relative beach face gradient for each beach-state (after Wright and Short, 1984). Indicative values of Ω are from Short (1999).

Figure 1

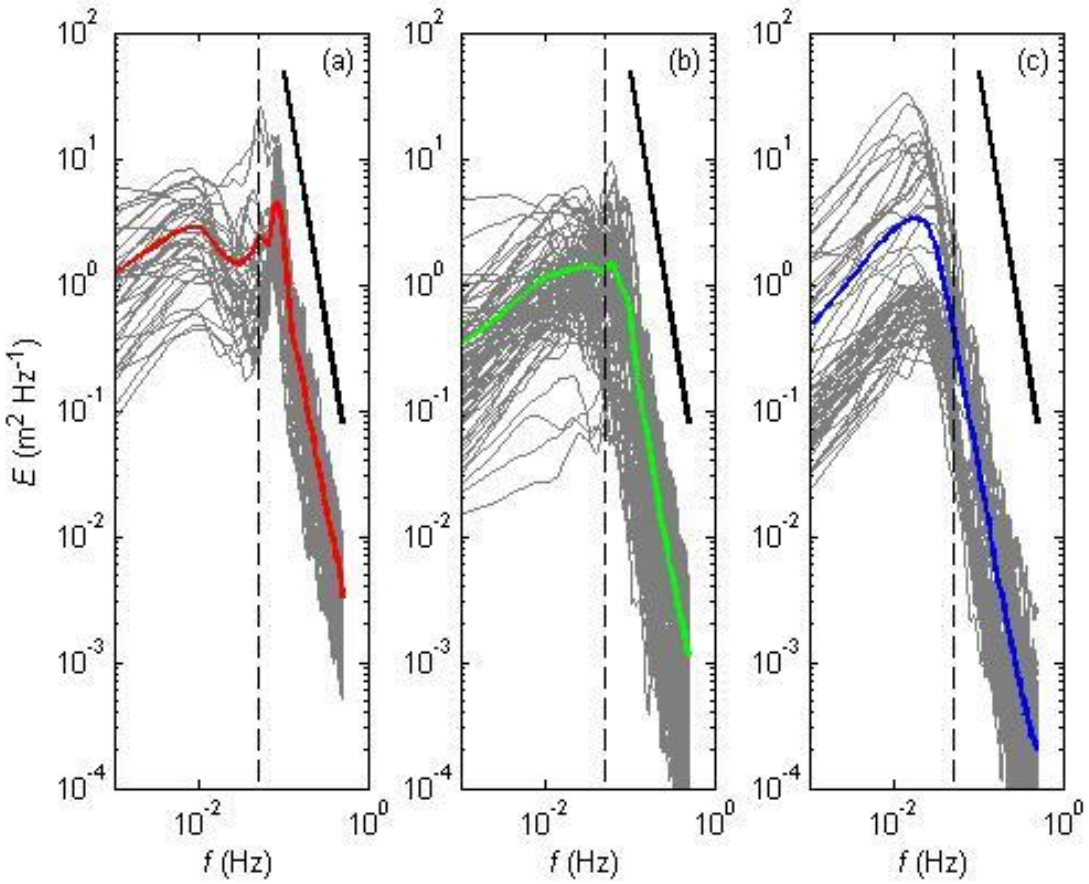

Figure 2

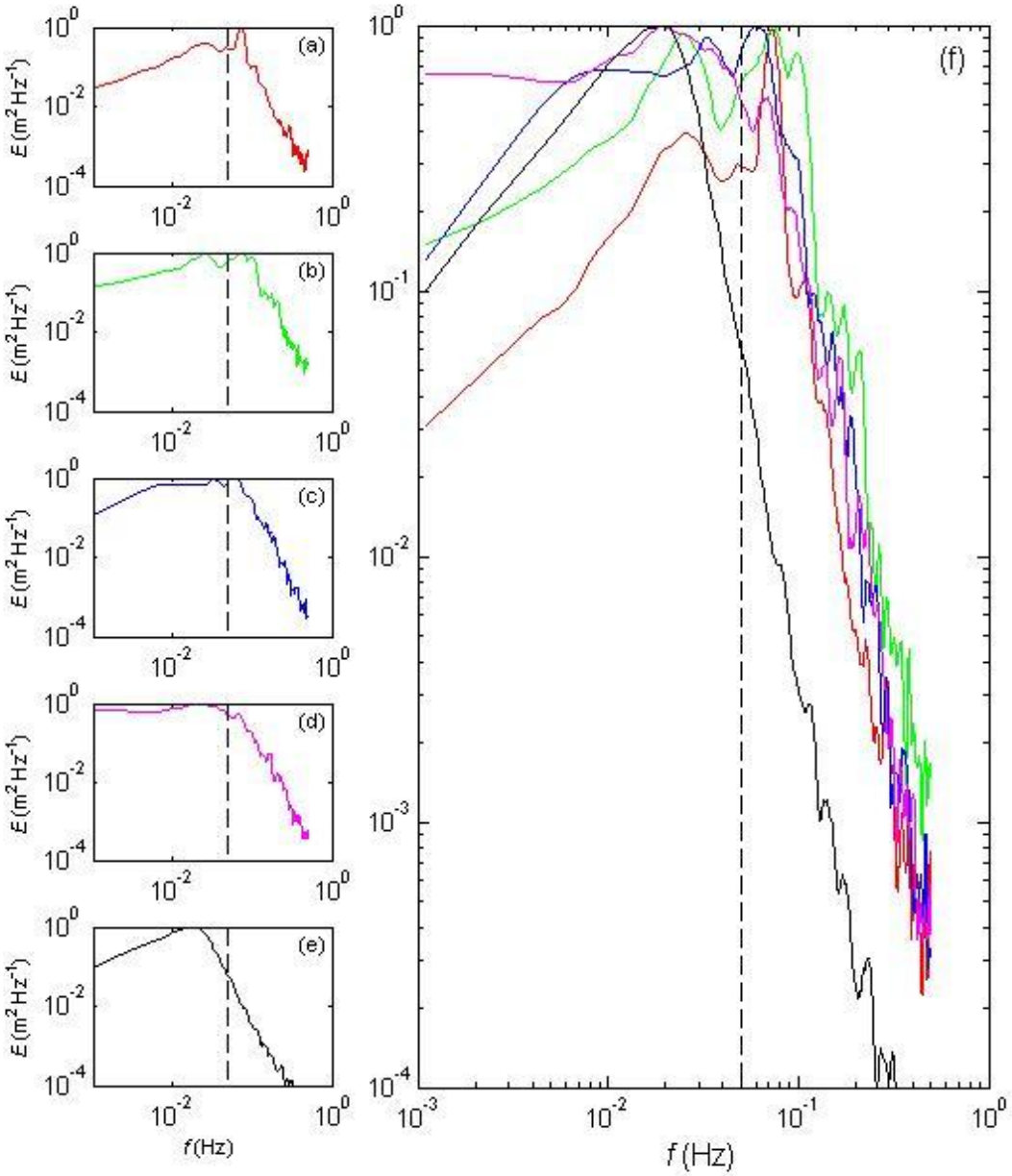

Figure 3

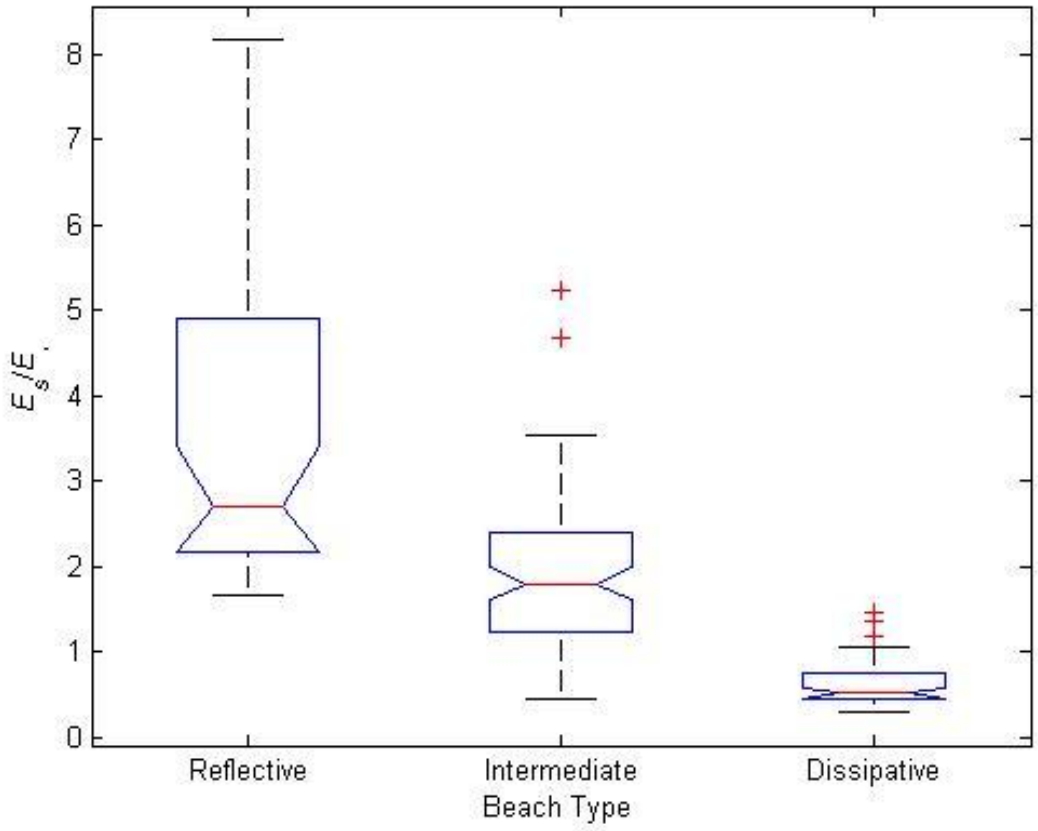

Figure 4

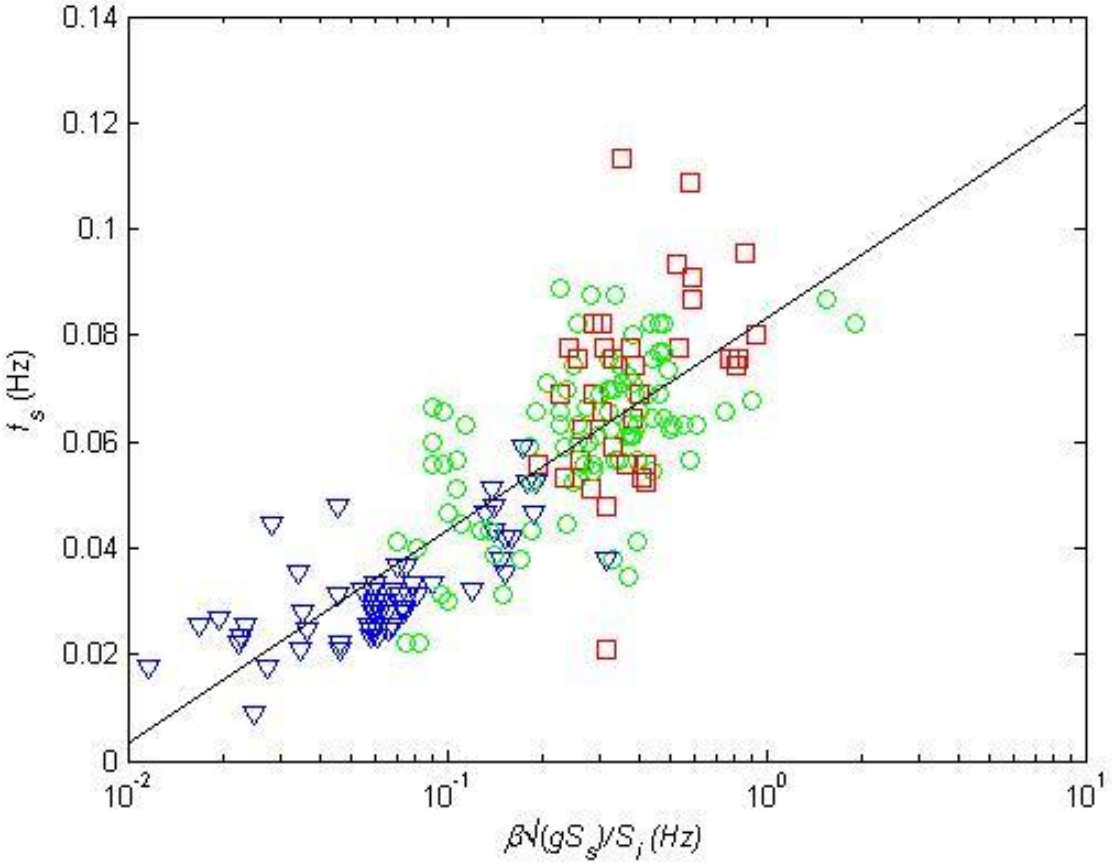

Figure 5

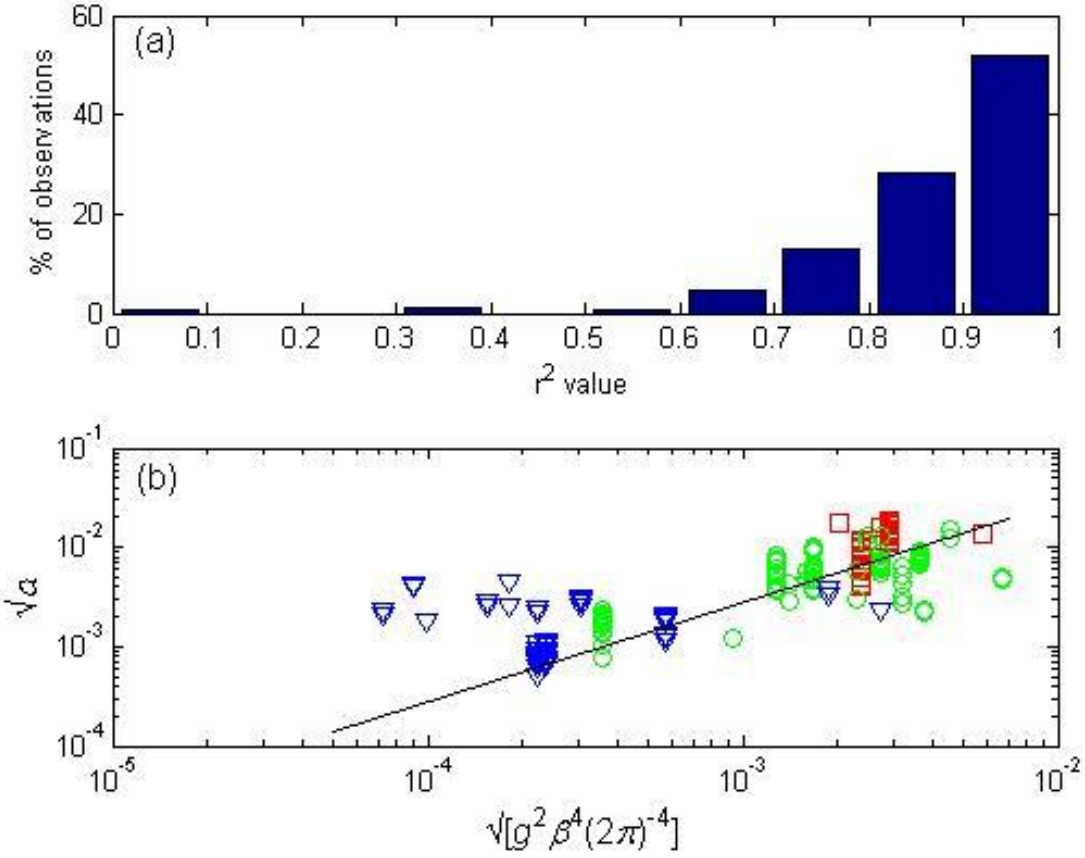

Figure 6

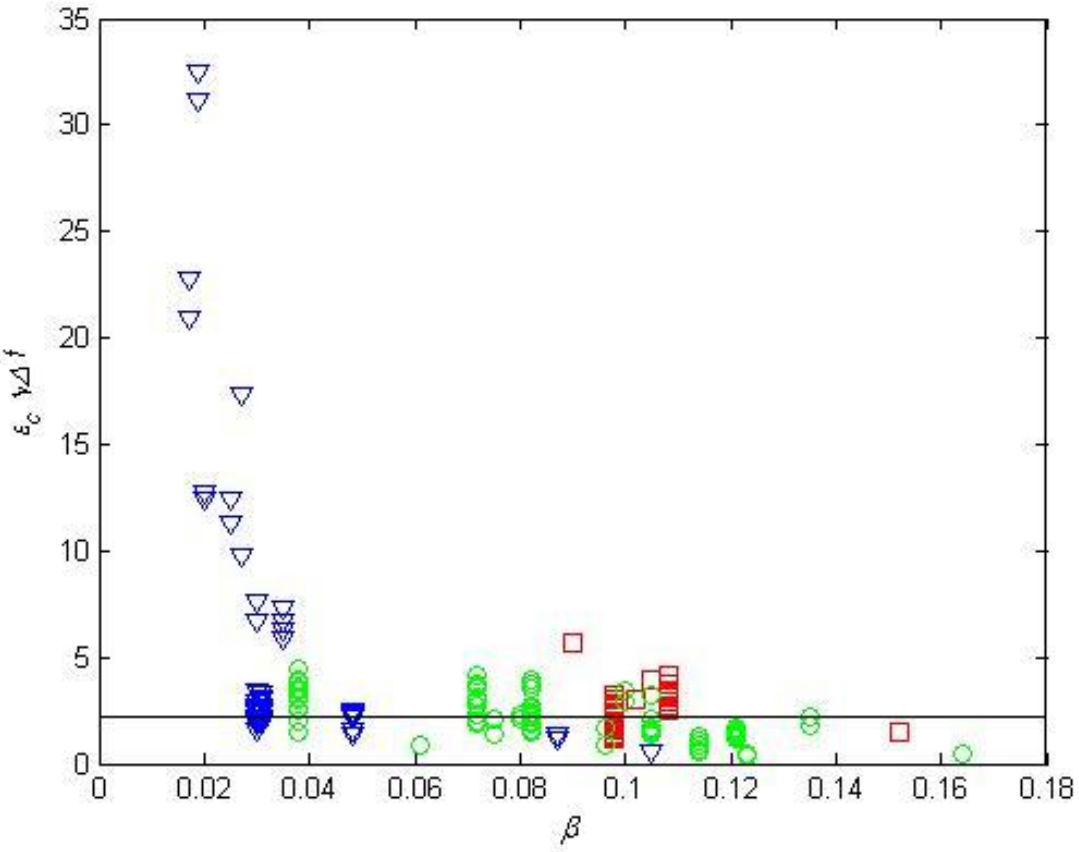

Figure 7

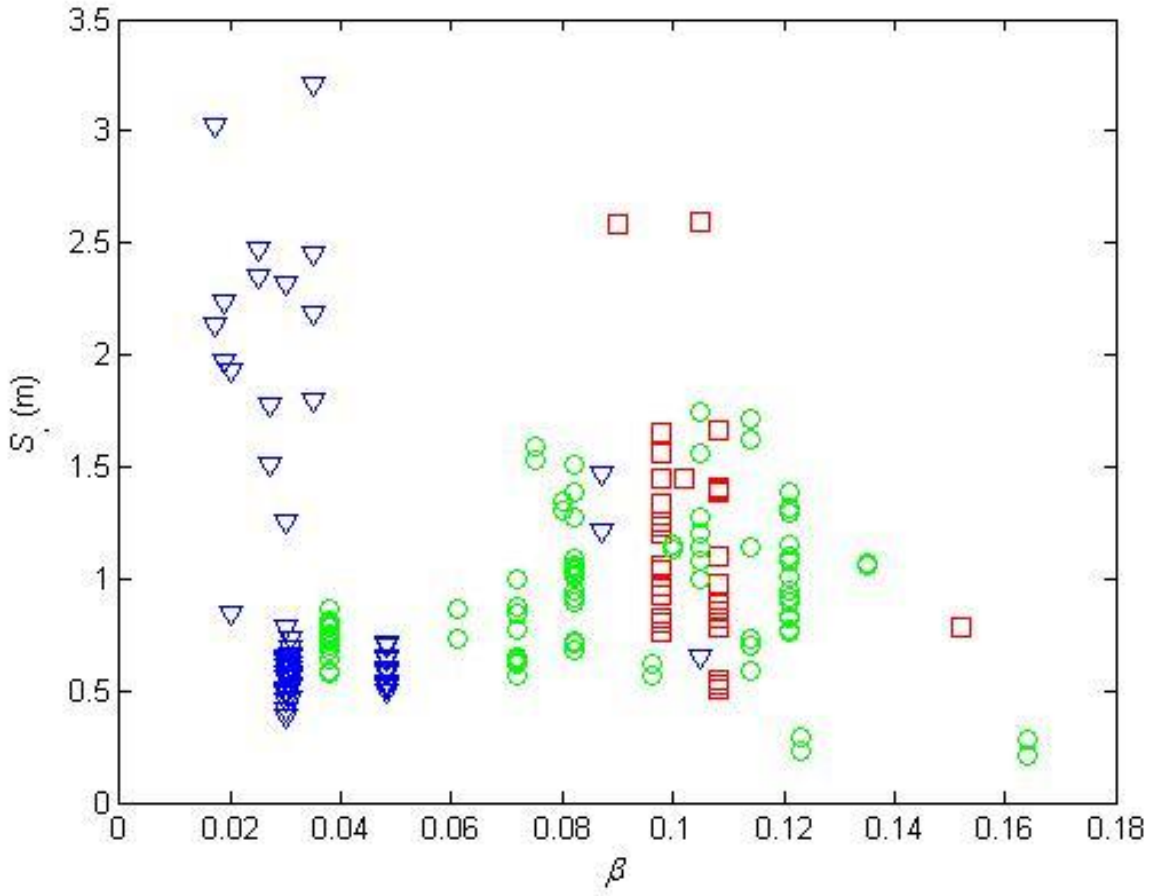

Figure 8

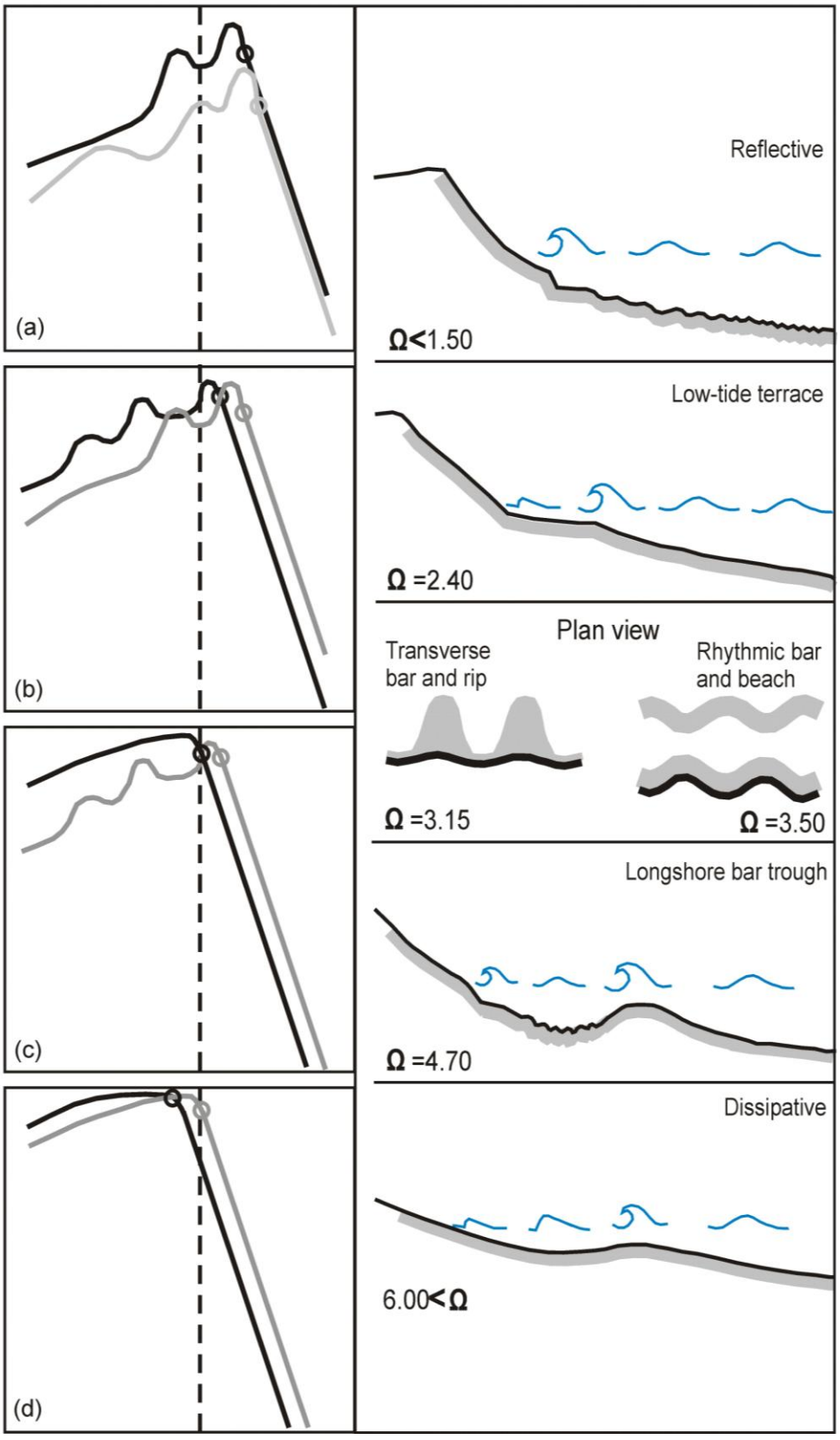

Highlights

Ratio of swash energy in the short and long wave bands varies with beach state.
Several other features of swash spectra scale with beach face gradient.
Morphodynamic controls on swash behaviour and spectral characteristics identified.
Swash spectral signatures incorporated into the morphodynamic beach state model.